Non-Propagating Components of Surface Electromyogram Reflect Motor Unit Firing Rates

Received July 13, 2019, accepted July 24, 2019, date of publication July 29, 2019, date of current version August 15, 2019.

Digital Object Identifier 10.1109/ACCESS.2019.2931609

Non-Propagating Components of Surface Electromyogram Reflect Motor Unit Firing Rates

LUCA MESIN
Mathematical Biology and Physiology, Dipartimento di Elettronica e Telecomunicazioni, Politecnico di Torino, 10129 Turin, Italy
e-mail: luca.mesin@polito.it

ABSTRACT Interference surface electromyogram (EMG) recorded from linear electrode arrays aligned to muscle fibres can be separated into propagating and non-propagating contributions. The first reflects the propagation of action potentials along muscle fibres. The non-propagating components are here shown to be related to the overall firing pattern of active motor units (MU). Indeed, in simulations, the power spectral density (PSD) of non-propagating components shows a low frequency peak corresponding to the mean firing rate, even when such a contribution is not visible in the PSD of the EMG (either monopolar or single differential configuration, either rectified or not). Moreover, it has a high correlation with the PSD of the cumulative firings of the MUs in the detection volume of the recording system. Applications to experimental data confirm that the low frequency peak is more evident for the non-propagating components than for the raw signals and is related to the MU firing frequency. Potential future applications are expected in the study of the MU control in different conditions (e.g., training, fatigue or pathology, inducing changes, or modulation of firing rate) and in the investigation of common synaptic inputs to motor neurons.

INDEX TERMS End-of-fibre effect, motor unit firing rate, non-propagating components, surface EMG.

I. INTRODUCTION

Surface electromyogram (EMG) reflects the bioelectric command inducing muscle contraction, providing information both on the peripheral adaptations of motor units (MU) and on their control. The mean MU firing rate (FR) was studied to extract information on MU control and its variations induced by fatigue [1]–[3], training [4], [5] or pathology [6], [7].

The power spectral density (PSD) of surface EMG reflects many properties of the active MUs. Theoretical [8]–[10] and experimental [11], [12] works suggested that the low frequency portion (under about 40 Hz) is mainly affected by the firing statistics, whereas, at higher frequencies, the PSD reflects the average shapes of MU action potentials (MUAPs). Separating the two contributions is important to focus on either central control or peripheral information. For example, in fatiguing contractions, a reduction of muscle fibre conduction velocity (CV) is associated to a proportional shrink of the portion of PSD reflecting MUAP shapes toward lower frequency. The low frequency peak is not directly affected by CV and was found to introduce problems in following CV variations by the study of simple spectral descriptors, like the median frequency [11]. This suggested using the shift in the midfrequency region of the EMG amplitude spectrum to better follow possible changes in CV [13].

However, the low frequency peak was not clearly visible in the PSD of all EMGs. For example, in [14] the occurrence of the peak was about in the 70% and 30% of the investigated cases, for frontalis and buccinators muscles, respectively. The relative weight of the peak was found to decrease with force, until being not visible for contraction levels higher than 40% of the maximal voluntary contraction (MVC) [15]. The absence of the low frequency peak was interpreted as reflecting large fluctuations of MU FR or poor reliability of PSD estimation, due to the short epochs investigated [14]. The shape of the intracellular action potential [16] and non-stationary contractions [17] can also affect the low frequency contributions of the spectrum.

To emphasize the low frequency peak reflecting MU FR, rectification of surface EMG was suggested [18], but some works criticized the method [19], [21]. As an alternative, neural strategies can be studied in detail by separating the interference data into the sum of single MU contributions by advanced decomposition methods [4], [5];

The associate editor coordinating the review of this manuscript and approving it for publication was Ruqiang Yan.

however, this solution is computationally intensive and requires high-density recordings [20].

A recent work proposed a robust and fast technique to split interference monopolar surface EMG into propagating and non-propagating contributions [22]. Separating the two contributions could be useful to focus on the properties of each of them. The identification of the propagating contribution was found to be useful to improve the estimation of muscle fibre CV [22]. Here, the non-propagating component is shown to include a low frequency peak in the PSD reflecting MU firing statistics, opening perspectives in the study of neuromuscular control, through the estimation of the average MU FR and its possible variations or modulations in physiology and pathology.

II. METHODS

A. SIMULATED DATA

A volume conductor model was used to simulate single fibre action potentials (SFAP). Specifically, the volume conductor was cylindrical [23] with a bone of 20 mm radius, skin of 1 mm thickness, superficial muscle with thickness of 15 mm. The fat layer was either 3 or 7 mm, generating two datasets. The muscle fibres had length and location of innervation zone (IZ) randomly chosen with a range of variation of 10 mm; in the average, they were symmetric with respect to the IZ, with 60 mm of mean semi-length. A linear array of four square electrodes (surface 1 mm^2) with inter-electrode distance (IED) of 10 mm was placed over the skin, aligned to the fibres and centred between the IZ and one tendon. Monopolar SFAPs were simulated and sampled at 2048 Hz.

Simulated fibre density was 20/mm^2. The same fibres were included in different MUs with superimposed territory, introducing an approximation in simulating their MUAPs [22]. The size of MUs was distributed exponentially in the range of 15-300 fibres. The total number of simulated MUs was 400. Their locations were randomly chosen within the muscle with uniform distribution. CV of MUs was chosen with a Gaussian distribution with mean 4 m/s and standard deviation 0.3 m/s. Greater values of CV were assigned to larger MUs.

A MU recruitment model was used to simulate interference EMG [24]. The geometrical, physiological and recruitment parameters were chosen to simulate the vastus lateralis muscle.

Different force levels (range 5-100% MVC, step 5%) were considered in a preliminary test. Then, stationary epochs of interference EMGs at 80% of MVC of duration 10 s were obtained, changing the following parameters.

1. MU CV distribution: it was changed by rescaling linearly the CVs of MUAPs distributed as indicated above; the mean was selected in the range 3-5 m/s (0.5 m/s step).

2. MU FR distribution with maximum FR (FR_{max}) in the range 20-40 Hz (with step 5 Hz) and minimum FR equal to $FR_{min} = 5$ Hz $+ 0.25\ FR_{max}$. It was obtained by changing linearly the FR distribution produced by the simulator of MU recruitment [24].

3. Inter-spike interval (ISI) variability: the coefficient of variation (COV) was either 10% or 20%.

Thus, in total, the number of considered signals was $100 = 5$ (CV distributions) $\times$ 5 (different FR) $\times$ 2 (fat thickness) $\times$ 2 (COV of ISI).

B. EXPERIMENTAL DATA

Different experimental signals were considered as example applications. A surface EMG from thenar muscle was taken from the dataset of a previous study [25]. The medial linear array of electrodes (silver circular electrodes, with contact area 0.8 mm^2, IED of 3 mm) aligned to the muscle fibres was selected from the 2D grid of 60 electrodes used in that study. The contraction level was kept around 6% MVC. A signal of duration 30 s was processed.

Other data were taken from the dataset of a study on vastus lateralis and medialis [26] (at 20% and 40% MVC, respectively). Linear adhesive arrays of eight, silver bar electrodes (1×10 mm, IED of 10 mm) were used. They were obtained from 10 s portions of bursts of activity arbitrarily selected from the dataset.

Digital second-order notch filters were applied off-line to remove power line interference at 50 Hz and the first 3 harmonics. Moreover, a high-pass filter removed low frequency artefacts (Chebyshev filter of type 2, order 3, cut-off frequency at 2 Hz; both filters were used twice, once with time reversed, to remove phase distortion and delay).

For each of the above mentioned data, an automatic algorithm was used to select the 4 monopolar channels from which the best propagation of single differential (SD) signals were obtained (i.e., maximum correlation with average signal obtained after alignment). A validated algorithm [27] was used to identify the firing trains of different MUs from the interference EMGs, considering all available electrodes.

C. SIGNAL PROCESSING

Propagating and non-propagating components were estimated from monopolar EMG using a recently proposed method [22], based on the iteration of two steps.

1. The propagating component is estimated by optimally mutually aligning all channels and by averaging across them. Then, the propagating term in each channel is computed from the estimated component by optimal time shifting and amplitude scaling.

2. The estimated propagating components are subtracted from all channels and the non-propagating part is obtained by averaging across them.

The estimated components were subtracted in each iteration, with amplitude computed optimally in each channel (in the least square sense). Largest non-propagating components were also removed and substituted by interpolation to improve the estimation of propagating signals (as detailed in [22]).

The PSD of non-propagating components was estimated by Welch method, considering sub-epochs of 0.5 s, overlap of 50% and zero padding in order to get 1 Hz resolution. It was

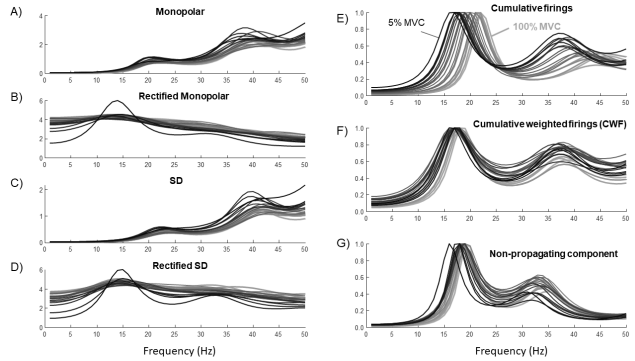

FIGURE 1. PSD of different signals in the low frequency range for increasing force levels (20 levels between 5% and 100% MVC, with lighter grayscale lines indicating larger force levels; fat layer thickness of 7 mm, coefficient of variation –COV– of the inter-spike interval –ISI– equal to 10%). A) Monopolar, B) rectified monopolar, C) single differential (SD), D) rectified SD, E) cumulative firings of active MUs, F) cumulative weighted firings (CWF; firings weighted by MUAP amplitudes), G) non-propagating component. Traces shown in A-D normalized by the standard deviation of the PSDs, those in E-G by their maximum.

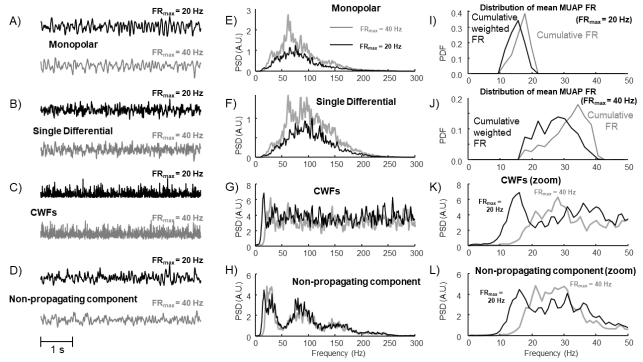

FIGURE 2. Examples of EMGs simulated with high force level (80% MVC) and different MU firing patterns, reflecting either a low or a high maximal firing rate (FR_{max} ; fat thickness 7 mm, COV of ISI 10%). A) Portion of the monopolar signal from the second electrode, corresponding to simulations with either of the two maximal FRs. B) Same as A), but showing the second SD channel. C) CWF. D) Non-propagating component (averaged across the 4 channels). E)-H) PSD of the signals shown in A)-D), respectively. I)-J) Probability density function (PDF) of mean FR of the MUs, for FR_{max} = 20 Hz and 40 Hz, respectively. K)-L) Same as G)-H), respectively, but showing the low frequencies (below 50 Hz) for an easier comparison with the distribution of FRs shown in I) and J).

compared to that of cumulative weighted firings (CWF), defined as the sum of the firings of active MUs multiplied by the average root mean square (RMS) of their MUAPs detected on the channels. This weighting procedure made it possible to take into account for the detection volume of the recording system. In fact, the MUAPs with greater amplitude provide a more energetic contribution to both the recorded EMG and its components (and also to their PSDs).

III. RESULTS

A. LOW FREQUENCY PEAK FOR DIFFERENT FORCE LEVELS

Preliminary tests are considered in Figure 1, showing the PSDs of simulated EMG at different force levels (only in this case, the PSD was obtained by the Burg method of order 100, which allowed to obtain single clear low frequency peaks).

The low frequency peak was less visible in the EMGs (monopolar or SD, either rectified or not) as the force level increased. On the other hand, the low frequency peak was always visible in the PSD of the non-propagating components. It translates towards higher mean frequencies as the force level increases with a variation similar to that of the PSD of CWF. Such variations are smaller than those found on the cumulative firings, as they are weighted by the amplitude of the MUAPs, which are statistically larger for big MUs just recruited and firing at small FRs.

B. HIGH FORCE LEVEL WITH DIFFERENT FIRING RATES

As the literature and the previous figure indicate that it is more difficult to find the low frequency peak on raw data (possibly filtered or rectified) considering increasing force levels, from now on simulations of a high force level (i.e., 80% MVC) are considered.

Figure 2 shows some examples of signals in time and frequency domain. Notice that the monopolar and SD signals do not show a clear peak in their PSDs corresponding to the mean FR. On the contrary, the PSD of the CWF shows a peak at low frequency (Figure 2K) that corresponds to the distribution of mean FR of the MUs within the detection volume (Figures 2I and 2J for two values of maximal FR, respectively). The distributions of mean FR have maximum for large values of FR, as most MUs are firing at their maximal frequency. However, the largest MUs are the last to be recruited and, at the simulated force level, they are firing at lower frequency. For this reason, the CWF distributions show peaks at lower frequencies than the distributions of mean FRs. Non-propagating component has a PSD including a low frequency peak, which reflects such an information (Figure 2L). In addition to such a peak, the PSDs of both CWF and non-propagating component show oscillations, reflecting the stochasticity of firing patterns and the harmonics of the low frequency peak. The shown PSDs of the CWF and non-propagating components have a correlation of 93.0% and 88.6% for maximal FR equal to 20 Hz and 40 Hz, respectively (correlation computed in the frequency range from 0 to FR_{max}+10 Hz).

Figure 3 shows the mean PSDs of CWF and non-propagating components obtained by averaging conditions with same maximal FR. The FR distributions are also shown (Figure 3C). The PSD of the CWF (Figure 3A) has a peak that translates together with the peak of the distribution of MU FRs (Figure 3C). The PSDs of the non-propagating components (Figure 3B) show also peaks that resemble those of the distribution of the CWF (Figure 3C).

C. THE CENTROID OF LOW FREQUENCY PEAK REFLECTS MEAN FR

Figure 4 shows that the centroid of the low frequency peak of the PSD of non-propagating components can be used to measure the mean FR. The local peaks of the PSD were first computed within the range 4-45 Hz, imposing a prominence

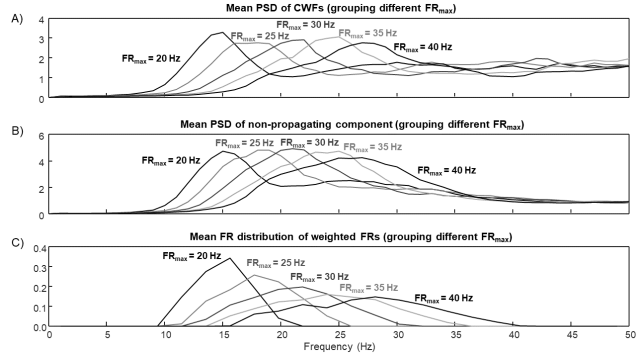

FIGURE 3. Mean PSDs (normalized by their standard deviation) and PDFs of simulated FRs obtained by averaging across 20 cases (corresponding to 2 fat layer thicknesses, 5 values of mean CV and 2 COVs of ISI), each with constant MU FR distribution. Both the CWF (A) and the non-propagating components (B) show peaks with location and spread which resemble those of the simulated weighted FR distributions (C).

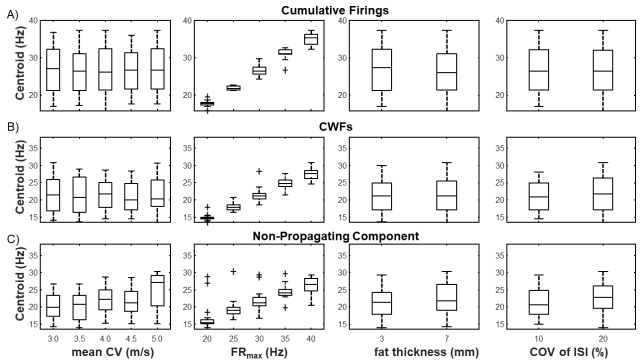

FIGURE 4. Location of the low frequency peak of the PSD of A) cumulative firings, B) CWF and C) non-propagating component. The estimated centroid of the low frequency peaks are given in terms of distributions (median, quartiles and range, with outliers shown individually) of values obtained by splitting with respect to different means of MU CV distributions, maximal FR, fat layer thickness and COV of ISI.

larger than 10% and a width of at least 4 Hz. Then, the one corresponding to the lowest frequency was selected as providing information on MU FRs. Nearby peaks, moving to higher frequencies, were also included in the set of interest if they were close to the previously selected peak (not more distant than 4 Hz) and high (not smaller than the 70% of the height of the previous peak). Once identified in this way the range of frequency including local peaks of the PSD possibly reflecting MU FRs, the range was further extended of 4 Hz in both directions. The PSD was then investigated in the resulting range of frequency, by estimating its centroid and spread (i.e., the standard deviation of the PSD in the selected frequency range). The same routine was applied to the PSDs of the cumulative firings of active MUs, the CWF and the non-propagating components. Only a few outliers can be noticed in Figure 4, indicating that the above-mentioned routine is quite stable. Notice that the low frequency peak of the cumulative firings reflects the mean FR of simulated MUs. The weighted firings are biased by the largest MUs, which have a lower FR than small MUs early recruited.

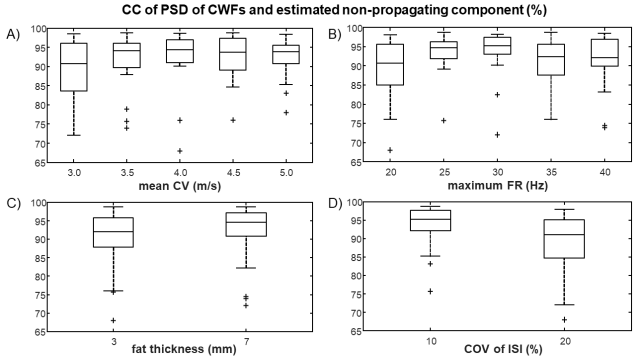

FIGURE 5. Distributions of correlation coefficients (CC) of the PSD of CWF and non-propagating component in the low frequency range (defined from 0 to the mean plus 3 times the standard deviation of the peak identified below 50 Hz). The CCs are split with respect to A) different mean CV of MUs, B) maximal FR, C) thickness of the fat layer and D) COV of ISI.

The centroid of the PSD of non-propagating components, even showing larger variability, fairly represents the information included in the CWF. The centroid of the cumulative firings (either weighted or not) is not affected by the simulated mean CV, fat layer thickness and COV of ISI. The estimation of non-propagating components is affected by the simulation parameters (as better shown by Figure 5, commented below): for example, the two components are more difficult to separate if the propagating one is faster (larger dispersion of centroid of the low frequency peak is obtained for a mean CV of 5 m/s with respect to lower values).

D. LOW FREQUENCY PEAK OF NON-PROPAGATING COMPONENTS TO STUDY MU FRs

Figure 5 shows that the low frequency components of the estimated non-propagating term correlate with those of the CWF. The correlation coefficient was computed considering the PSDs (of CWF and non-propagating components) in the frequency range [0 - C±3·S], where C and S indicate centroid and spread of non-propagating components, respectively. Notice that a larger median of the distribution of correlation coefficients is found for a thicker fat layer, as, in that case, non-propagating components are more evident, so that they are simpler to be estimated (Wilcoxon signed rank test significant, $p < 0.05$). Moreover, as expected, lower correlations are obtained in the average if the COV of ISI is larger, as the low frequency peak of the PSD has a larger spread (Wilcoxon signed rank test highly significant, $p << 0.01$).

E. TESTS ON EXPERIMENTAL DATA

Figure 6 shows applications to different experimental data. In the case of the small level contraction of the thenar muscle shown in Figure 6A, a small low frequency peak is found at about 10 Hz in the PSD of monopolar and SD EMG (Figure 6D). A larger peak at the same frequency is found in the PSDs of CWF and non-propagating components (Figure 6G).

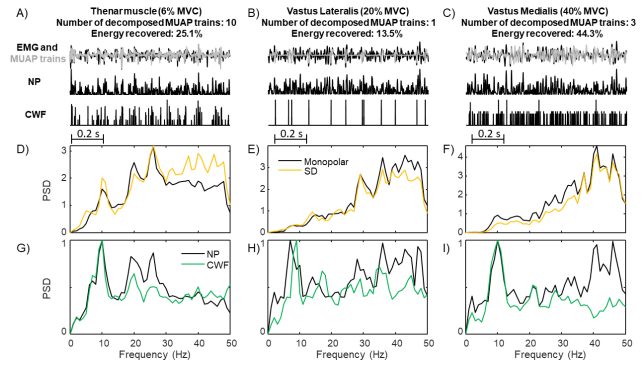

FIGURE 6. Test on experimental data from A) thenar muscle, B) vastus lateralis and C) vastus medialis (30 s, 10 s and 10 s of stationary contractions, respectively). EMG was decomposed: the indicated numbers of MUAP trains were identified, accounting for a portion of the energy of the original data. The low frequency portion of the PSDs of monopolar and SD data (normalized with respect to their standard deviation) are shown in D), E) and F), for thenar, vastus lateralis and medialis muscles, respectively. The corresponding PSDs of the non-propagating component (NP) and CWF are shown in G), H) and I) (normalization with respect to the low frequency peak amplitude).

For larger contraction levels (20% and 40% MVC, for vastus lateratis and medialis, respectively), no evident low frequency peak is found in the PSD of the EMG (Figures 6E and 6F). On the other hand, it emerges in the PSDs of CWF and non-propagating components (Figures 6H and 6I; notice that the two peaks are a bit different in the case of the vastus lateralis, but, in such a case, a single MUAP train was identified, accounting only for a small portion of the total energy of the signal).

IV. DISCUSSION

The control of MUs is affected by many conditions, including different exerted force levels [8], adaptation to muscle fatigue [1]–[3], training [4], [5] and pathology [6], [7]. Furthermore, the coupling in specific frequency ranges of signals reflecting the activity of either different muscles [28] or the brain and a muscle [29] may provide precise information on possible synergies [30] or control deficits [31].

Until now, the study of MU FR from surface EMG has been based on either simple methods relying on the raw signal, possibly after rectification [18]–[21], or computationally intensive algorithms decomposing the data into the contributions of single MUs [4], [5]. However, simple techniques still have problems in processing EMG at high force levels [19] and decomposition algorithms may require many electrodes to distinguish different MUAP shapes [20] and account only for a portion of the energetic content of the data (e.g., EMG energies recovered for the data shown in Figure 6 were about 25%, 13% and 44% of the total, respectively). Moreover, an efficient method for EMG decomposition (based on a 5-pin surface EMG system) was found to provide results contradicting well-established knowledge, like as the common drive [32], so that only some methods (recording data from many channels [20]) could be able to replicate the findings derived from intramuscular recordings [33].

Here, a simple and stable method is proposed, which was able to show a low frequency peak reflecting mean MU FR even under high force levels, when the PSD of the raw signal (possibly filtered or rectified) did not (Figure 1). The low frequency peak was sensitive to the simulated MU FR modulations, even at a high force level (80% MVC; Figures 2 and 3).

The variations of the low frequency peak in simulations were found to be small (in line with previous experimental observations [14]). Indeed, the information is weighted by the amplitudes of MUAPs, which are in the average greater for larger MUs, which are the last to be recruited and are firing at a rate that is lower than their maximum. As shown in Figures 4 and 5, the information provided by the PSD of the estimated non-propagating components is equivalent to that of the CWF (weighting MUAPs to account for the detection volume of the recording system).

The method is based on strong assumptions. Only generation and extinction of action potentials contributed to non-propagating components of simulated EMGs. In real signals, common mode interference (e.g., due to movement artefacts or power line) could make more difficult to extract clear information (however, movement artefacts and power line interfere at a lower and higher frequency range, respectively, than that of the average MU firing rate). Moreover, propagating components should have same shape across channels. However, different CVs of active MUs induce variations. Moreover, additional possible shape variations derive from the misalignment of the electrode array with respect to the muscle fibres [34]. This could influence negatively the estimation of the two components. However, preliminary tests on the same simulations discussed in [22] show that the method is stable to a misalignment of 20°. Additional problems are tissue in-homogeneity [23], not rectilinear muscle fibres or going deep in the muscle [35], multiple IZs (hence, different directions of MUAP propagation [36], [37]). In all these conditions, the modelling assumptions of the method are not satisfied, so that its reliability is questionable. An interesting case is that of pinnate muscles with fibres going deep: the superficial aponeurosis makes the extinction of the potential very evident. Some preliminary tests on simulation (based on the model discussed in [35]) proves that the low frequency peak is found in the raw data even at 80% MVC. A more evident low frequency peak was found on the estimated non-propagating components, showing that, even in such conditions, the algorithm was able to correctly remove some propagating contributions.

It is also worth noticing that non-propagating components have a large detection volume, which improves representativeness. This means that they provide overall information on the muscle of interest, instead of being selective to the activity of a small region [38]. However, this property makes them prone to crosstalk.

Some applications on real data are shown in Figure 6. A decomposition algorithm [27] extracted some information on MU firings. The PSDs of non-propagating components

always showed a low frequency peak (even at high force levels when it was not visible from the PSD of the data). Such a peak was consistent with the one found in the PSD of CWF of the few MUs identified by the decomposition algorithm.

The promising results shown here should be tested further in experiments. Intramuscular EMG or high-density surface EMG could be decomposed to better investigate the possibility of extracting information on the MU firing patterns by the proposed method, which only requires non-invasive recordings from few electrodes. Moreover, the significance of the method could be tested based on the reliability of information extracted in different applications, e.g., in the study of FR modulation under different conditions. For example, a pair of indices was suggested to discriminate among peripheral and central manifestations of myoelectric fatigue [2], [3]. Fractal dimension was found to reflect MU firing behaviour [2], but could not discriminate between synchronization and mean FR [3]. By exploring the spectrum (or other properties) of non-propagating components, more information could be extracted.

Additional applications could be in the fields of coherence [28] and common drive [39] by investigating possible coupling among non-propagating components estimated from EMG recorded in different locations. Notice that the highest and most uniform spatial distribution of cortex-muscle coherence was found in [25] when considering monopolar instead of differential derivations. The Authors of [25] suggested that non-propagating components (preserved in monopolar data) contributed to a better estimation of coherence, due to their larger detection volume and reduced phase cancellation. More investigation of this hypothesis is now possible, as non-propagating components could be separated and used to estimate coherence.

V. CONCLUSION

Non-propagating components have been largely removed in the literature, e.g., to reduce crosstalk or the bias in CV estimation. This paper shows that separating propagating and non-propagating contributions of surface EMG can be useful, as both components provide interesting information. Specifically, non-propagating components provide information on MU discharges. Their estimation can be achieved using a simple EMG recording system with few electrodes [22], opening potential applications in studies in which simple recording systems are used (in line with a recent work proposing another method to investigate cumulative MU firings from single channel EMG [40]).

ACKNOWLEDGMENTS

Experimental data were provided by LISiN (Laboratorio di Ingegneria del Sistema Neuromuscolare e della riabilitazione motoria, Turin, Italy). Decomposition of experimental EMGs was performed by A. Botter and T.M. Vieira.

REFERENCES

[1] L. McManus, X. Hu, W. Z. Rymer, M. M. Lowery, and N. L. Suresh, "Changes in motor unit behavior following isometric fatigue of the first dorsal interosseous muscle," *J. Neurophysiol.*, vol. 113, no. 9, pp. 3186–3196, 2015.

[2] L. Mesin, C. Cescon, M. Gazzoni, R. Merletti, and A. Rainoldi, "A bi-dimensional index for the selective assessment of myoelectric manifestations of peripheral and central muscle fatigue," *J. Electromyogr. Kinesiol.*, vol. 19, no. 5, pp. 851–863, 2009.

[3] L. Mesin, D. Dardanello, A. Rainoldi, and G. Boccia, "Motor unit firing rates and synchronisation affect the fractal dimension of simulated surface electromyogram during isometric/isotonic contraction of vastus lateralis muscle," *Med. Eng. Phys.*, vol. 38, no. 12, pp. 1530–1533, 2016.

[4] H. L. Dimmick, J. D. Miller, A. J. Sterczala, M. A. Trevino, and T. J. Herda, "Vastus lateralis muscle tissue composition and motor unit properties in chronically endurance-trained vs. sedentary women," *Eur. J. Appl. Physiol.*, vol. 118, no. 9, pp. 1789–1800, 20188.

[5] A. J. Sterczala, J. D. Miller, M. A. Trevino, H. L. Dimmick, and T. J. Herda, "Differences in the motor unit firing rates and amplitudes in relation to recruitment thresholds during submaximal contractions of the first dorsal interosseous between chronically resistance-trained and physically active men," *Appl. Physiol., Nutrition, Metabolism*, vol. 43, no. 8, pp. 759–768, 2018.

[6] L. McManus, X. Hu, W. Z. Rymer, N. L. Suresh, and M. M. Lowery, "Motor unit activity during fatiguing isometric muscle contraction in hemispheric stroke survivors," *Frontiers Hum. Neurosci.*, vol. 11, p. 569, Nov. 2017.

[7] P. Y. Dikmen, E. K. Orhan, and M. B. Baslo, "Analysis of motor unit firing characteristics in patients with motor neuron diseases," *Somatosensory Motor Res.*, vol. 33, no. 1, pp. 16–19, 2016.

[8] J. Basmajian and C. J. De Luca, *Muscles Alive: Their Function Revealed by Electromyography*, 5th ed. Baltimore, MD, USA: Williams & Wilkins, 1985.

[9] C. J. De Luca, "Physiology and mathematics of myoelectric signals," *IEEE Trans. Biomed. Eng.*, vol. BME-26, no. 6, pp. 313–325, Jun. 1979.

[10] R. S. Le Fever and C. J. De Luca, "The contribution of individual motor units to the EMG power spectrum," in *Proc. 29th Annu. Conf. Eng. Med. Biol.*, Boston, MA, USA, 1976, p. 16.

[11] A. van Boxtel and L. R. B. Schomaker, "Influence of motor unit firing statistics on the median frequency of the EMG power spectrum," *Eur. J. Appl. Physiol. Occupational Physiol.*, vol. 52, no. 2, pp. 207–213, 1984.

[12] A. Van Boxtel, "Optimal signal bandwidth for the recording of surface EMG activity of facial, jaw, oral, and neck muscles," *Psychophysiology*, vol. 38, no. 1, pp. 22–34, 2001.

[13] M. M. Lowery, C. L. Vaughan, P. J. Nolan, and M. J. O'Malley, "Spectral compression of the electromyographic signal due to decreasing muscle fiber conduction velocity," *IEEE Trans. Rehabil. Eng.*, vol. 8, no. 3, pp. 353–361, Sep. 2000.

[14] A. Van Boxtel and L. R. B. Schomaker, "Motor unit firing rate during static contraction indicated by the surface EMG power spectrum," *IEEE Trans. Biomed. Eng.*, vol. BME-30, no. 9, pp. 601–609, Sep. 1983.

[15] P. J. Lago and N. B. Jones, "Low-frequency spectral analysis of the e.m.g," *Med. Biol. Eng. Comput.*, vol. 19, no. 6, pp. 779–782, 1981.

[16] G. V. Dimitrov and N. A. Dimitrova, "Fundamentals of power spectra of extracellular potentials produced by a skeletal muscle fibre of finite length Part II: Effect of parameters altering with functional state," *Med. Eng. Phys.*, vol. 20, no. 9, pp. 702–707, 1998.

[17] K. B. Englehart and P. A. Parker, "Single motor unit myoelectric signal analysis with nonstationary data," *IEEE Trans. Biomed. Eng.*, vol. 41, no. 2, pp. 168–180, Feb. 1994.

[18] L. J. Myers, M. M. Lowery, M. O'Malley, C. L. Vaughan, C. Heneghan, A. S. C. Gibson, Y. X. R. Harley, and R. Sreenivasan, "Rectification and non-linear pre-processing of EMG signals for cortico-muscular analysis," *J. Neurosci. Methods*, vol. 124, no. 2, pp. 157–165, 2003.

[19] D. Farina, R. Merletti, and R. M. Enoka, "The extraction of neural strategies from the surface EMG," *J. Appl. Physiol.*, vol. 96, no. 4, pp. 1486–1495, 2004.

[20] D. Farina, R. Merletti, and R. M. Enoka, "The extraction of neural strategies from the surface EMG: An update," *J. Appl. Physiol.*, vol. 117, no. 11, pp. 1215–1230, 2014.

[21] O. P. Neto and E. A. Christou, "Rectification of the EMG signal impairs the identification of oscillatory input to the muscle," *J. Neurophysiol.*, vol. 103, no. 2, pp. 1093–1103, Dec. 2009.

[22] L. Mesin, "Separation of interference surface electromyogram into propagating and non-propagating components," *Biomed. Signal Process. Control*, vol. 52, pp. 238–247, Jul. 2019.
[23] L. Mesin, "Volume conductor models in surface electromyography: Computational techniques," *Comput. Biol. Med.*, vol. 43, no. 7, pp. 942–952, 2013.
[24] P. Contessa and C. J. De Luca, "Neural control of muscle force: Indications from a simulation model," *J. Neurophysiol.*, vol. 109, pp. 1548–1570, Dec. Dec. 2013.
[25] H. Piitulainen, A. Botter, M. Bourguignon, V. Jousmäki, and R. Hari, "Spatial variability in cortex-muscle coherence investigated with magnetoencephalography and high-density surface electromyography," *J. Neurophysiol.*, vol. 114, no. 5, pp. 2843–2853, 2015.
[26] L. M. L. de Souza, H. V. Cabral, L. F. de Oliveira, and T. M. Vieira, "Motor units in vastus lateralis and in different vastus medialis regions show different firing properties during low-level, isometric knee extension contraction," *Hum. Movement Sci.*, vol. 58, pp. 307–314, Apr. 2018.
[27] A. Holobar and D. Zazula, "Multichannel blind source separation using convolution kernel compensation," *IEEE Trans. Signal Process.*, vol. 55, no. 9, pp. 4487–4496, Sep. 2007.
[28] S. N. Baker, J. M. Kilner, E. M. Pinches, and R. N. Lemon, "The role of synchrony and oscillations in the motor output," *Exp. Brain Res.*, vol. 128, nos. 1–2, pp. 109–117, 2007.
[29] B. A. Conway, D. M. Halliday, S. F. Farmer, U. Shahani, P. Maas, A. I. Weir, and J. R. Rosenberg, "Synchronization between motor cortex and spinal motoneuronal pool during the performance of a maintained motor task in man," *J. Physiol.*, vol. 489, no. 3, pp. 917–924, 1995.
[30] C. J. De Luca and Z. Erim, "Common drive in motor units of a synergistic muscle pair," *J. Neurophysiol.*, vol. 87, no. 4, pp. 2200–2204, 2002.
[31] S. F. Farmer, M. Swash, D. A. Ingram, and J. A. Stephens, "Changes in motor unit synchronization following central nervous lesions in man," *J. Physiol.*, vol. 463, no. 1, pp. 83–105, 1993.
[32] M. Piotrkiewicz and K. S. Türker, "Onion skin or common drive?" *Front Cell Neurosci.*, vol. 11, p. 2, Jan. 2017.
[33] R. M. Enoka, "Physiological validation of the decomposition of surface EMG signals," *J. Electromyogr. Kinesiol.*, vol. 46, pp. 70–83, Jun. 2019.
[34] C. Cescon, P. Rebecchi, and R. Merletti, "Effect of electrode array position and subcutaneous tissue thickness on conduction velocity estimation in upper trapezius muscle," *J. Electromyogr. Kinesiol.*, vol. 18, no. 4, pp. 628–636, Aug. 2008.
[35] L. Mesin, R. Merletti, and T. M. Vieira, "Insights gained into the interpretation of surface electromyograms from the gastrocnemius muscles: A simulation study," *J. Biomech.*, vol. 44, no. 6, pp. 1096–1103, 2011.
[36] L. Mesin, L. Damiano, and D. Farina, "Estimation of average muscle fiber conduction velocity from simulated surface EMG in pinnate muscles," *J. Neurosci. Methods*, vol. 160, pp. 327–334, Mar. 2007.
[37] M. Nielsen, T. Graven-Nielsen, and D. Farina, "Effect of innervation-zone distribution on estimates of average muscle-fiber conduction velocity," *Muscle Nerve*, vol. 37, no. 1, pp. 68–78, 2008.
[38] T. M. Vieira, A. Botter, S. Muceli, and D. Farina, "Specificity of surface EMG recordings for gastrocnemius during upright standing," *Sci. Rep.*, vol. 7, no. 1, 2017, Art. no. 13300.
[39] C. J. de Luca and Z. Erim, "Common drive of motor units in regulation of muscle force," *Trends Neurosci.*, vol. 17, no. 7, pp. 299–305, 1994.
[40] L. Mesin, "Single channel surface electromyogram deconvolution to explore motor unit discharges," *Med. Biol. Eng. Comput.*, 2019.

LUCA MESIN graduated in electronics engineering, in 1999 and received the Ph.D. degree in applied mathematics from the Politecnico di Torino, Italy, in 2003, where he is currently an Associate Professor in biomedical engineering and a Supervisor of the Mathematical Biology and Physiology Group, Department of Electronics and Telecommunications. His current research interests include biomedical image and signal processing, and mathematical modeling.